Hydrodynamic model for particle beam-driven wakefield in MWCNTs*

Simulation of a photomultiplier tube**

AITANA

Student report: Pablo Martín-Luna

Email: pablo.martin@ific.uv.es

*Work in collaboration with NOVAS group (ICMUV)
**Work in collaboration with F. Hueso-González (IRIS group)

AITANA ANNUAL MEETING 2023 – MATTER & TECHNOLOGY
02 FEBRUARY 2024, VALENCIA, SPAIN

Contents (CNTs)

1. Introduction
2. Theoretical background
3. Results
4. Conclusions and outlook

1. Introduction

- The current state-of-the-art of the RF techniques for particle acceleration is limited to gradients on the order of 100 MV/m
- To obtain higher energies, we can increase the length of the accelerators... or use new techniques of acceleration with higher gradients

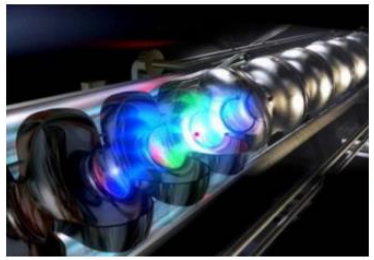

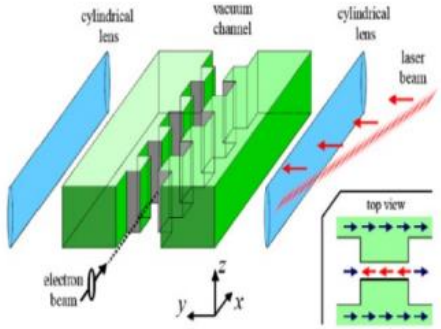

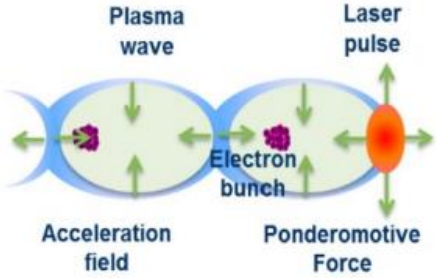

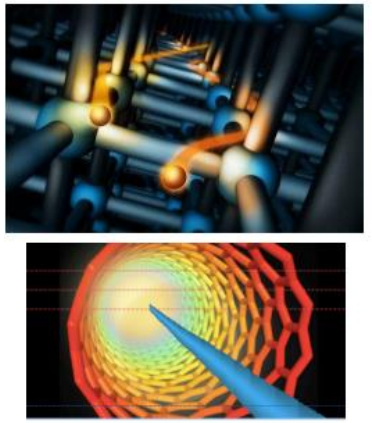

	Conventional RF cavities	Dielectric laser – driven acceleration (DLA)	Plasma / Laser wakefield acceleration (PWFA / LWFA)	Solid-state plasma wakefield acceleration
Based on	Normal / superconducting cavities	Quartz / silicon structure	Gaseous plasma	Crystals, nano-channels, CNTs
Max. longitudinal electric field	$\sim 100\ \mathrm{MV/m}$	$\sim 10\ \mathrm{GV/m}$	$\sim 100\ \mathrm{GV/m}$	$\sim 1 - 100\ \mathrm{TV/m}$ (prediction)
Limitation	Surface breakdown	Damage threshold	Wave breaking	Wave breaking

1. Introduction

- Plasma-based accelerators → GeV/cm accelerating gradients (wakefield amplitude ∝ plasma density):

$$E_0[\mathrm{V/m}] = \frac{m_e c \omega_p}{e} \approx 96\sqrt{n_0[\mathrm{cm^{-3}}]}$$

- Density of charge carriers in solids → 4–5 orders of magnitude higher than those in a gaseous plasma
- Solid-based acceleration media, such as crystals or nanostructures, could enable ultra-high gradients, on the order of E_0~ 1–10 TV/m

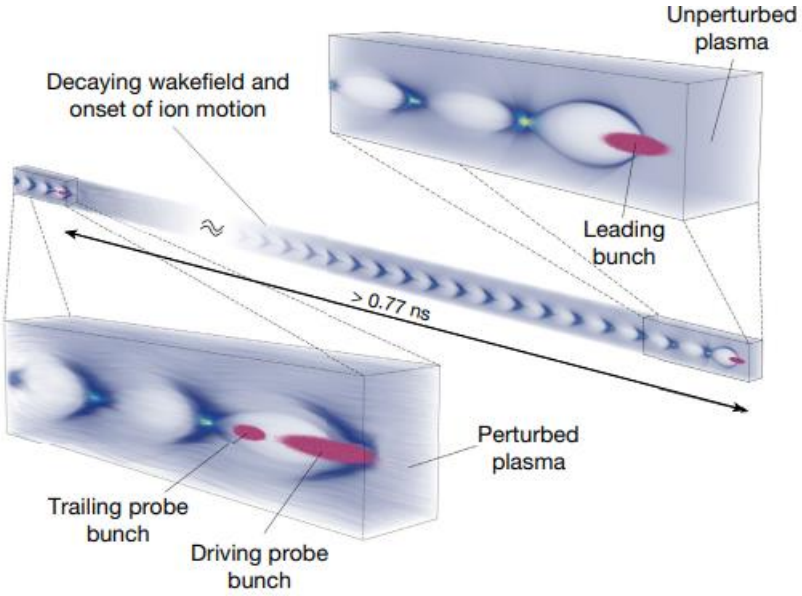

- If compared to natural crystals, 2D carbon-based structures could help achieving more realistic regimes:
  - larger dimensional flexibility / thermomechanical strength
  - transverse acceptances of up to ~100 nm (3 orders of magnitude higher than a typical silicon channel)
  - lower dechanneling rate
- 2D carbon-based materials (graphene, CNT) are good candidates to be used as ultra-compact accelerating structures

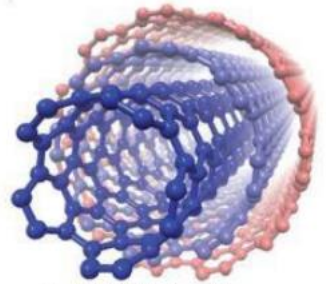

Multi-Walled carbon NanoTube (MWNT)

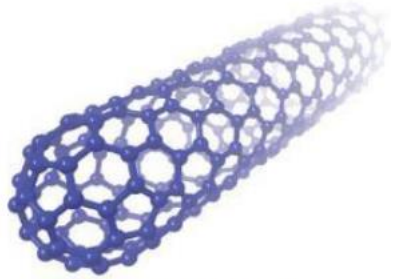

Single-Walled NanoTube (SWNT)

1. Introduction

- **Plasmonic acceleration**
  - Excitation of surface plasmonic modes by laser (laser-driven) or charged particle beam (beam-driven)
  - Collective motion of wall electrons acting like a structured plasma
  - To properly excite wakefields laser or beam driving parameters need to be in the time and space scale of the plasmon wave

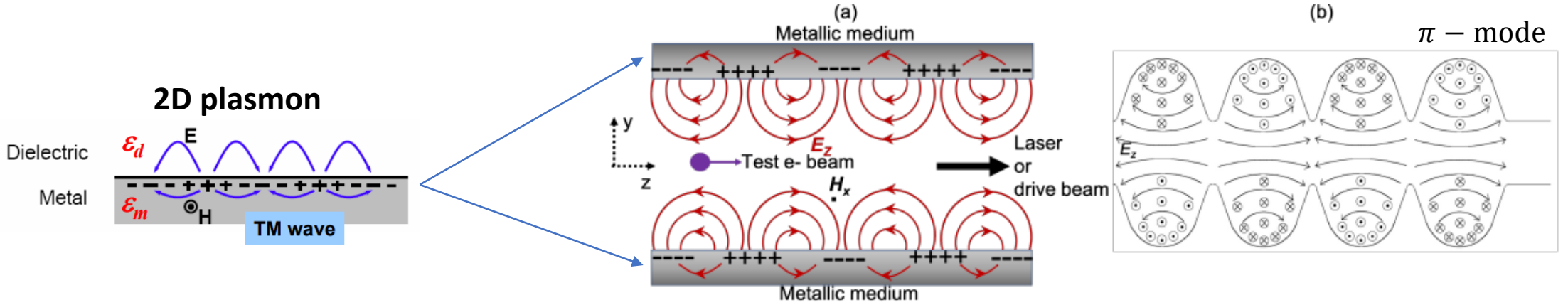

	Plasmonic acceleration	RF cavities
Aperture size	$\sim\mu$m	$\sim$cm
Length	$\sim$mm	~ 10cm − m
Longitudinal electric field	~ 100 GV/m	~ 100 MV/m
Operation	Travelling wave (TW)	Standing Wave (SW) or TW

2. Theoretical background

- **Geometry**
  - 2D electron gas confined in the cylindrical surface of a nanotube or microtube (made of CNTs, metallic nature)
  - Let us assume a point-like charge q travelling with speed v inside a carbon nanotube

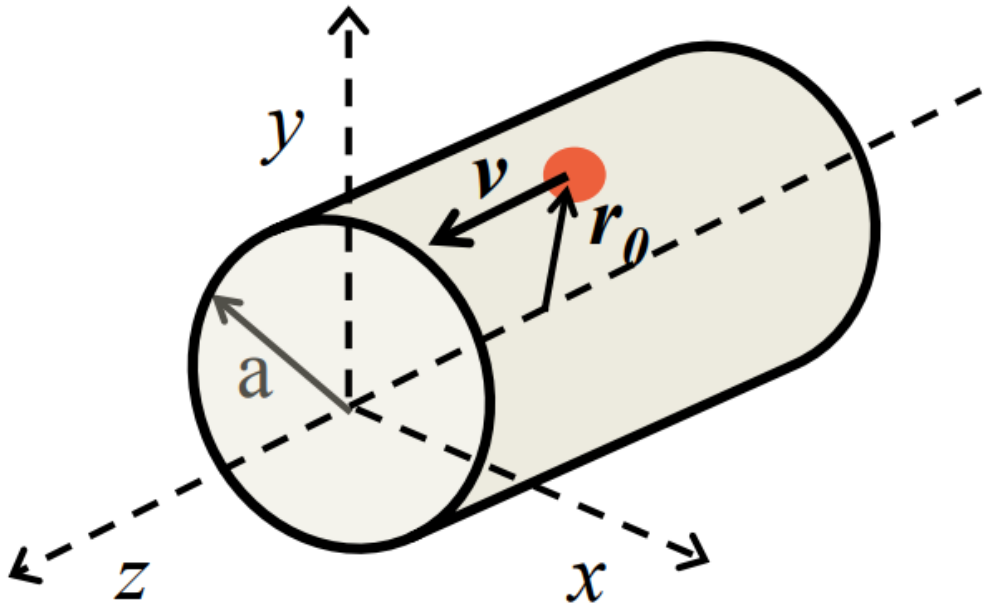

Driving charge at position:

$$\mathbf{r_0} = (\mathrm{r}_0, \varphi_0, z_0)$$

Position of electrons excited at the j-th surface:

$$\mathbf{r_{a,j}} = (\mathrm{a}, \varphi_a, z_a)$$

j-th wall: $n\left(\mathbf{r_{a,j}}, t\right) = n_0 + n_j(\mathbf{r_a}, t)$

Y-N. Wang, Z. L. Mišković, Phys. Rev. A 69 (2004) 022901
Z. L. Mišković et al., Phys. Lett. A 329 (2004) 94

2. Theoretical background

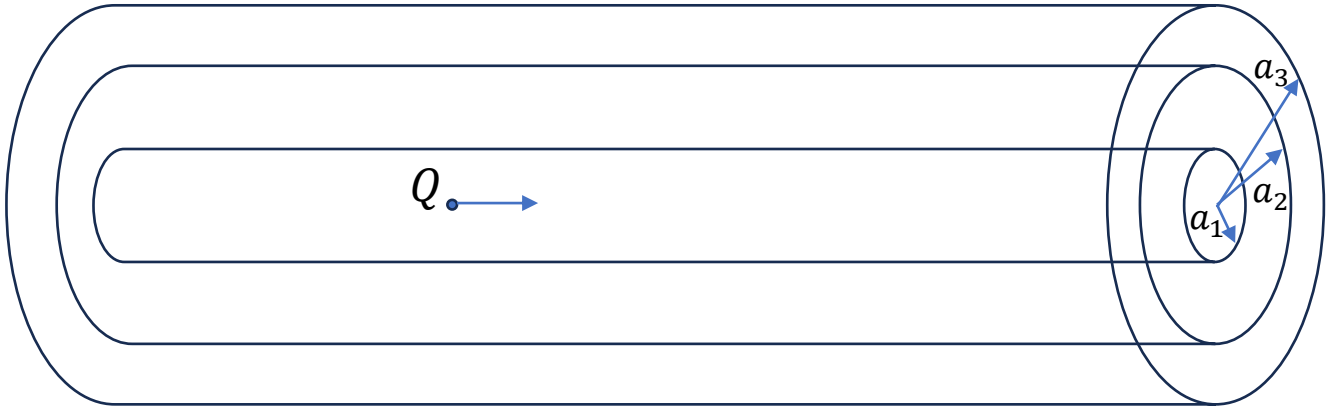

- Continuity eq for each wall:

(1)
$$\frac{\partial n_j(\mathbf{x}_j,t)}{\partial t}+n_0\nabla_j\cdot\mathbf{u}_j(\mathbf{x}_j,t)=0$$

- Momentum-balance eq for each wall:

(2)
$$\frac{\partial \mathbf{u}_j(\mathbf{x}_j,t)}{\partial t}=\nabla_j\Phi(\mathbf{x},t)|_{r=a_j}-\frac{\alpha}{n_0}\nabla_j n_j(\mathbf{x}_j,t)+\frac{\beta}{n_0}\nabla_j\left[\nabla_j^2 n_j(\mathbf{x}_j,t)\right]-\gamma\mathbf{u}_j(\mathbf{x}_j,t).$$

- The potential can be obtained by Poisson eq. Potential is: $\Phi=\Phi_{\text{ext}}+\Phi_{\text{ind}}$

(3)
$$\Phi_{\text{ind}}(\mathbf{x},t)=-\sum_l\int \mathrm{d}^2\mathbf{x}_l'\frac{n_l(\mathbf{x}_l',t)}{\|\mathbf{x}-\mathbf{x}_l'\|},\qquad \mathbf{x}_l'=\{a_l,\varphi',z'\}\qquad \mathrm{d}^2\mathbf{x}_l'=a_l\mathrm{d}\varphi'\,\mathrm{d}z'$$

Atomic units ared used thorought

2. Theoretical background

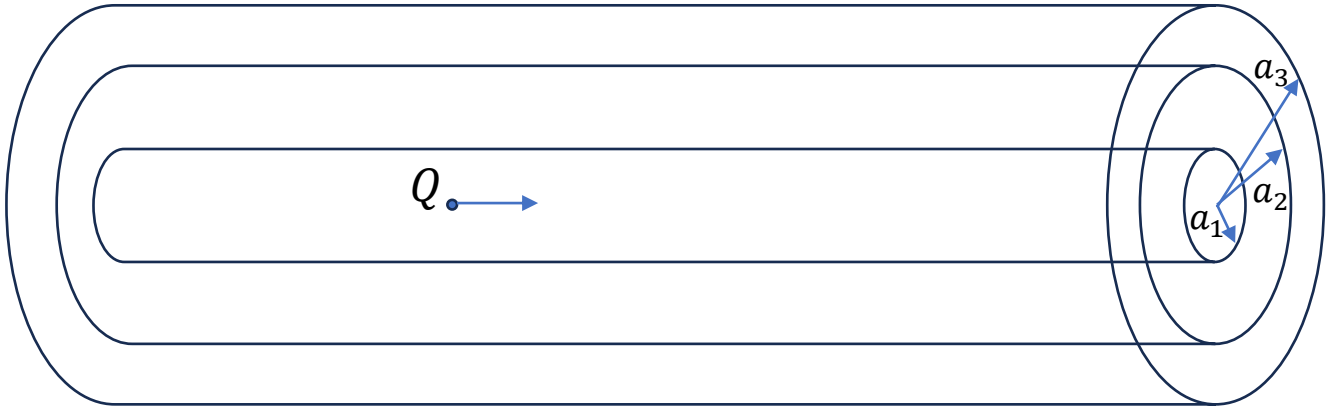

- Fourier-Bessel (FB) definition:

(4) $$A(\varphi,z,t)=\sum_{m=-\infty}^{\infty}\int_{-\infty}^{\infty}\frac{\mathrm{d}k}{(2\pi)^2}\int_{-\infty}^{\infty}\frac{\mathrm{d}\omega}{2\pi}\mathrm{e}^{\mathrm{i}kz+\mathrm{i}m\varphi-\mathrm{i}\omega t}\widetilde{A}(m,k,\omega)$$

- In particular:

(5) $$\frac{1}{\|\mathbf{x}-\mathbf{x}'\|}=\sum_{m=-\infty}^{\infty}\int_{-\infty}^{\infty}\frac{\mathrm{d}k}{(2\pi)^2}\mathrm{e}^{\mathrm{i}k(z-z')+\mathrm{i}m(\varphi-\varphi')}g(r,r';m,k),$$

$$g(r,r';m,k)\equiv 4\pi I_m(|k|r_<)K_m(|k|r_>)$$

$$r_<=\min(r,r') \qquad r_>=\max(r,r')$$

- From (3-5)

(6) $$\tilde{\Phi}_{\mathrm{ind}}(r,m,k,\omega)=-\sum_j g(r,a_j;m,k)a_j\tilde{n}_j(m,k,\omega),$$

2. Theoretical background

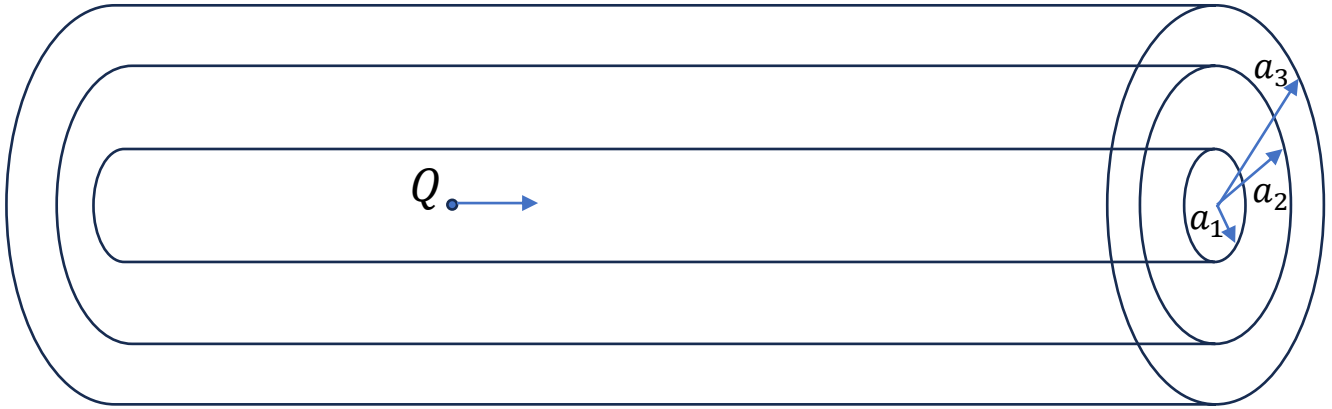

- From (1-2) and (6)

(7)
$$\left[\omega(\omega+\mathrm{i}\gamma)-\alpha\left(k^2+\frac{m^2}{a_j^2}\right)-\beta\left(k^2+\frac{m^2}{a_j^2}\right)^2\right]\tilde{n}_j(m,k,\omega)-\sum_l G_{jl}(m,k)\tilde{n}_l(m,k,\omega)=-n_0\left(k^2+\frac{m^2}{a_j^2}\right)\tilde{\Phi}_{\mathrm{ext}}(a_j,m,k,\omega),$$

$$G_{jl}(m,k)\equiv n_0 a_l\left(k^2+\tfrac{m^2}{a_j^2}\right)g(a_j,a_l;m,k).$$

$$\tilde{\Phi}_{\mathrm{ext}}(r,m,k,\omega)=Q\ 2\pi g(r,r_0;m,k)\delta(\omega-kv)\exp(-\mathrm{i}m\varphi_0)$$

- Eq (7) is a matrix eq: $A\vec{\tilde{n}}=\vec{b}$ When you have all the $\tilde{n}$, you can calculate $\tilde{\Phi}$ via (6) and make the FB (4) to obtain Φ.
- The relation det(A)=0 for j=2 (DoubleWCNT) gives the dispersion relation:

$$\omega_{\pm}^2=\frac{\omega_1^2+\omega_2^2}{2}\pm\sqrt{\left(\frac{\omega_1^2-\omega_2^2}{2}\right)^2+\Delta^2},$$

Individual dispersion relation for single CNT

$$\omega_j^2=\underbrace{\pi n_0}_{\alpha}(k^2+m^2/a_j^2)+\underbrace{\tfrac{1}{4}}_{\beta}(k^2+m^2/a_j^2)^2+n_0a_j(k^2+m^2/a_j^2)g(a_j,a_j;m,k)$$

Interaction term

$$\Delta^2=n_0^2a_1a_2(k^2+m^2/a_1^2)(k^2+m^2/a_2^2)g^2(a_1,a_2;m,k)$$

2. Theoretical background

- An example for $n_0 = n_g$, a $= 1$ nm (gap 1 nm),

Mode m=0

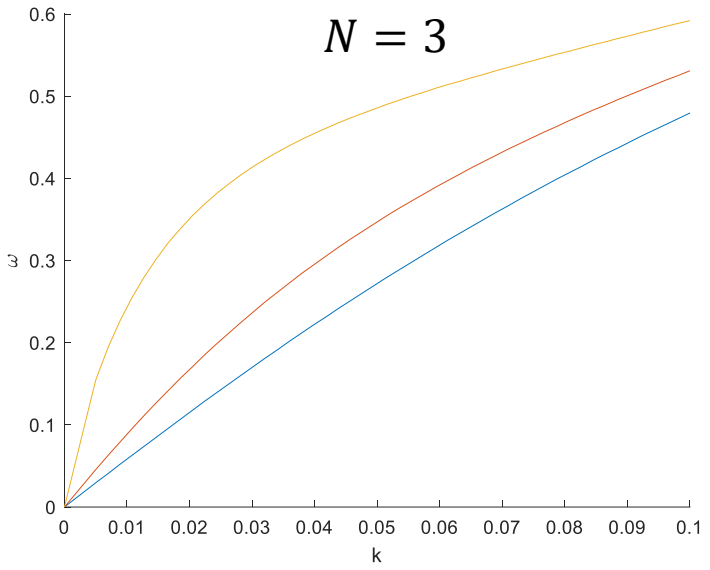

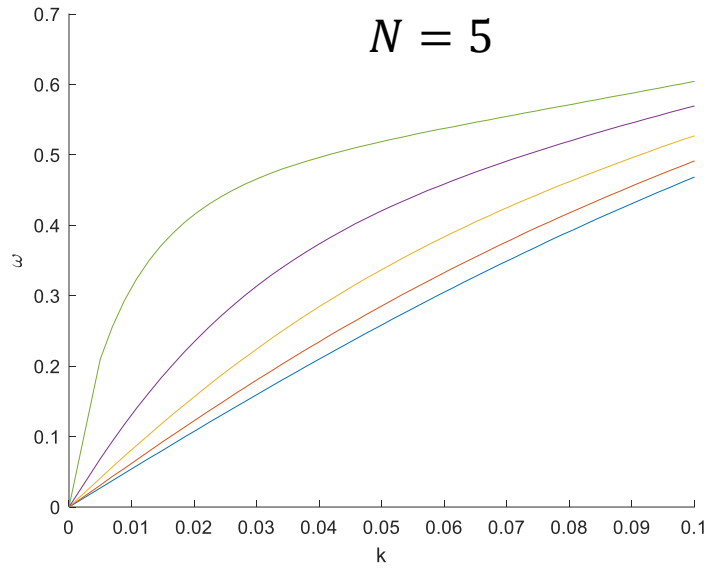

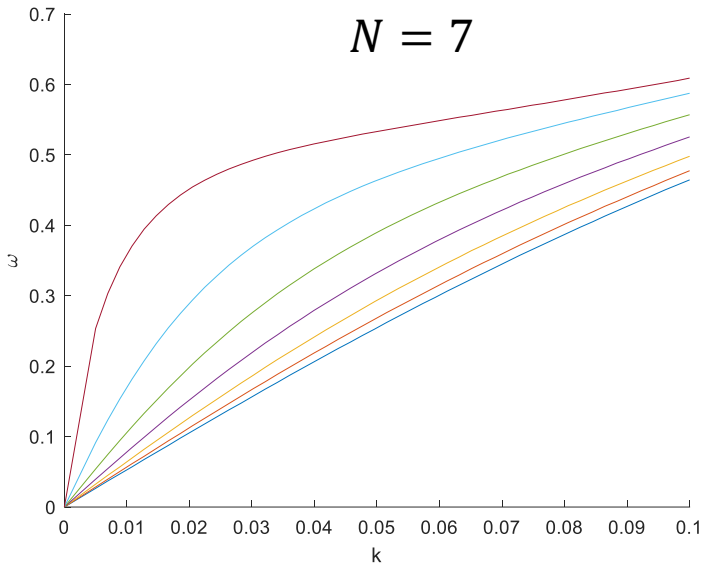

2. Theoretical background

- Excited wakefields

$$W_{z,\mathrm{ind}} = -\frac{\partial \Phi_{\mathrm{ind}}}{\partial z} = \frac{1}{(2\pi)^3}\sum_{m=-\infty}^{+\infty} e^{im\varphi}\int_{-\infty}^{+\infty} \mathrm{d}k\, k\left(\mathrm{Re}\left[\tilde{\Phi}_{\mathrm{ind}}(r,m,k,kv)\right]\sin(k\zeta) + \mathrm{Im}\left[\tilde{\Phi}_{\mathrm{ind}}(r,m,k,kv)\right]\cos(k\zeta)\right) = W_{z,\mathrm{Re}} + W_{z,\mathrm{Im}},$$

$$W_{r,\mathrm{ind}} = -\frac{\partial \Phi_{\mathrm{ind}}}{\partial r} = -\frac{1}{(2\pi)^3}\sum_{m=-\infty}^{+\infty} e^{im\varphi}\int_{-\infty}^{+\infty} \mathrm{d}k\,\left(\mathrm{Re}\left[\partial_r\tilde{\Phi}_{\mathrm{ind}}(r,m,k,kv)\right]\cos(k\zeta) - \mathrm{Im}\left[\partial_r\tilde{\Phi}_{\mathrm{ind}}(r,m,k,kv)\right]\sin(k\zeta)\right) = W_{r,\mathrm{Re}} + W_{r,\mathrm{Im}},$$

- The term that comes from the imaginary part can be analytically integrated if $\gamma \to 0^+$ for a SWCNT:

$$W_{z,\mathrm{Im}}(r,\varphi,\zeta) = \frac{-Q}{8\pi^2}\sum_{m=-\infty}^{+\infty} e^{im(\varphi-\varphi_0)} k_m \Omega_p^2 a^2 \left(k_m^2 + m^2/a^2\right) g\left(a, r_0; m, k_m\right) g\left(a, r; m, k_m\right) \left|\frac{\partial Z_m}{\partial k}\right|^{-1}_{k=k_m} \cos\left(k_m\zeta\right),$$

$$W_{r,\mathrm{Im}}(r,\varphi,\zeta) = \frac{-Q}{8\pi^2}\sum_{m=-\infty}^{+\infty} e^{im(\varphi-\varphi_0)} \Omega_p^2 a^2 \left(k_m^2 + m^2/a^2\right) g\left(a, r_0; m, k_m\right) \partial_r g\left(a, r; m, k_m\right) \left|\frac{\partial Z_m}{\partial k}\right|^{-1}_{k=k_m} \sin\left(k_m\zeta\right),$$

$$\Omega_p = \sqrt{4\pi n_0/a} \qquad Z_m(k) = (kv)^2 - \omega_m^2(k)$$

See: https://doi.org/10.1088/1367-2630/ad127c

https://doi.org/10.1088/1367-2630/ad127c

3. Results

- **Resonant frequencies:**

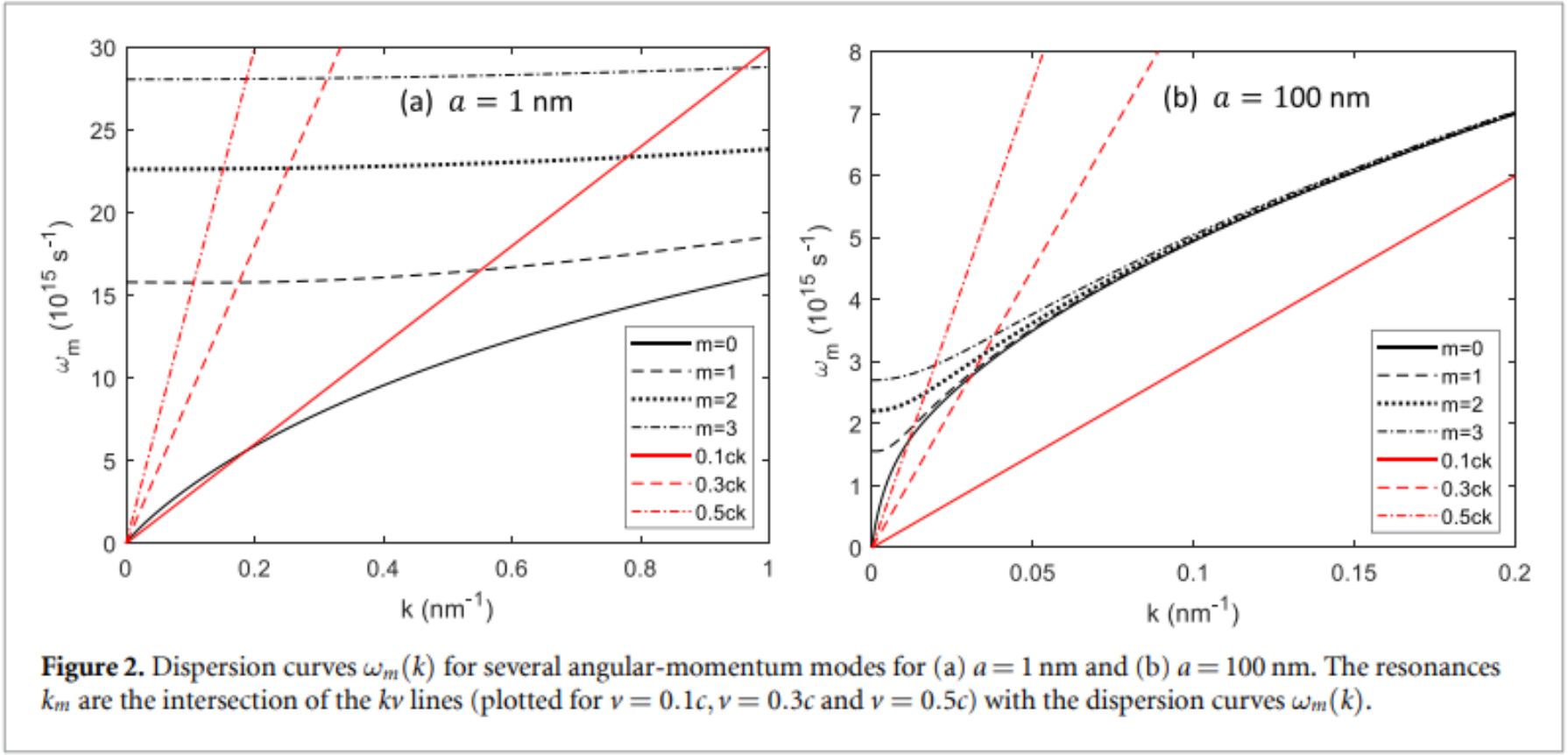

Figure 2. Dispersion curves $\omega_m(k)$ for several angular-momentum modes for (a) $a = 1$ nm and (b) $a = 100$ nm. The resonances k_m are the intersection of the kv lines (plotted for $v = 0.1c, v = 0.3c$ and $v = 0.5c$) with the dispersion curves $\omega_m(k)$.

For small CNT radius, high velocities may not excite the fundamental mode.

3. Results

- **Excited wakefields:**

The friction parameter γ produces an exponential decay of the wakefield.
It can be seen that: $W_{z,Re} \approx W_{z,Im}$ and consequently the expression in terms of the resonant frequencies may be used to approximate the wakefields.

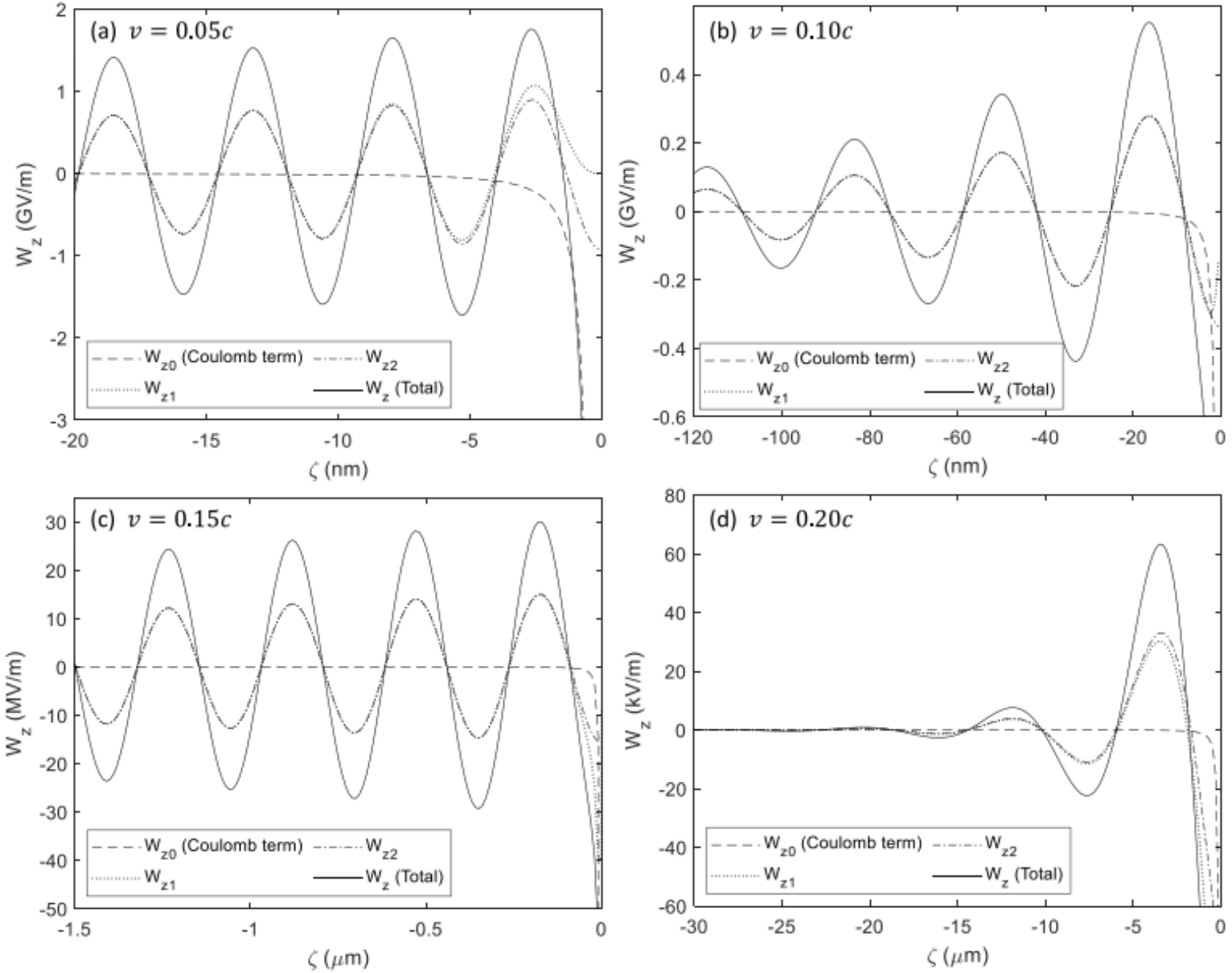

Figure 4. Longitudinal wakefield contributions on axis ($r = 0$) for a proton travelling on axis ($r_0 = 0$) at different velocity values: (a) $v = 0.05c$, (b) $v = 0.10c$, (c) $v = 0.15c$ and (d) $v = 0.20c$. The CNT radius is $a = 1$ nm and the friction parameter is $\gamma = 0.01\Omega_p$ in cases (a) and (b), and $\gamma = 0.0001\Omega_p$ in (c) and (d). Note that the driving proton is at $\zeta = 0$.

https://doi.org/10.1088/1367-2630/ad127c

https://doi.org/10.1088/1367-2630/ad127c

3. Results

- **Excited wakefields:**

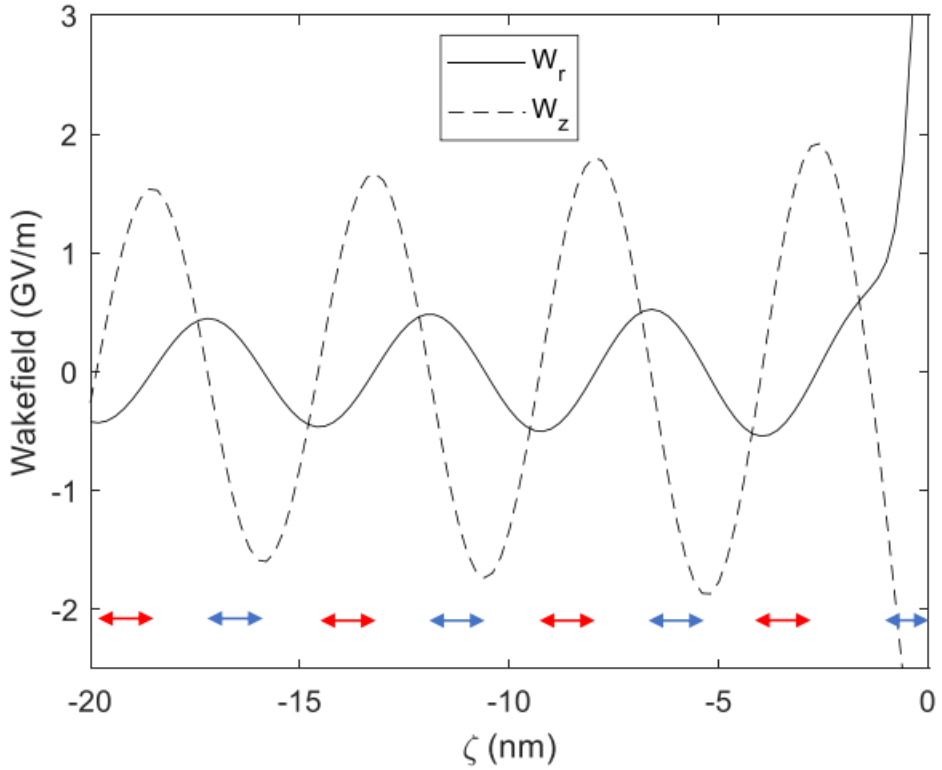

Figure 7. Wakefields (including the Coulomb term) at $r = a/2$ for $a = 1$ nm, $v = 0.05c$, $\gamma = 0.01\Omega_p$ and $r_0 = 0$. The red (blue) arrows indicate the regions where a positive (negative) witness charged particle would experience both acceleration and focusing simultaneously.

There are periodical regions where the witness charged particles can simultaneously experience both acceleration and focusing (if they travel off-axis)

https://doi.org/10.1088/1367-2630/ad127c

3. Results

- **Normalized units:**

$$\lambda_p = \frac{2\pi c}{\Omega_p}$$

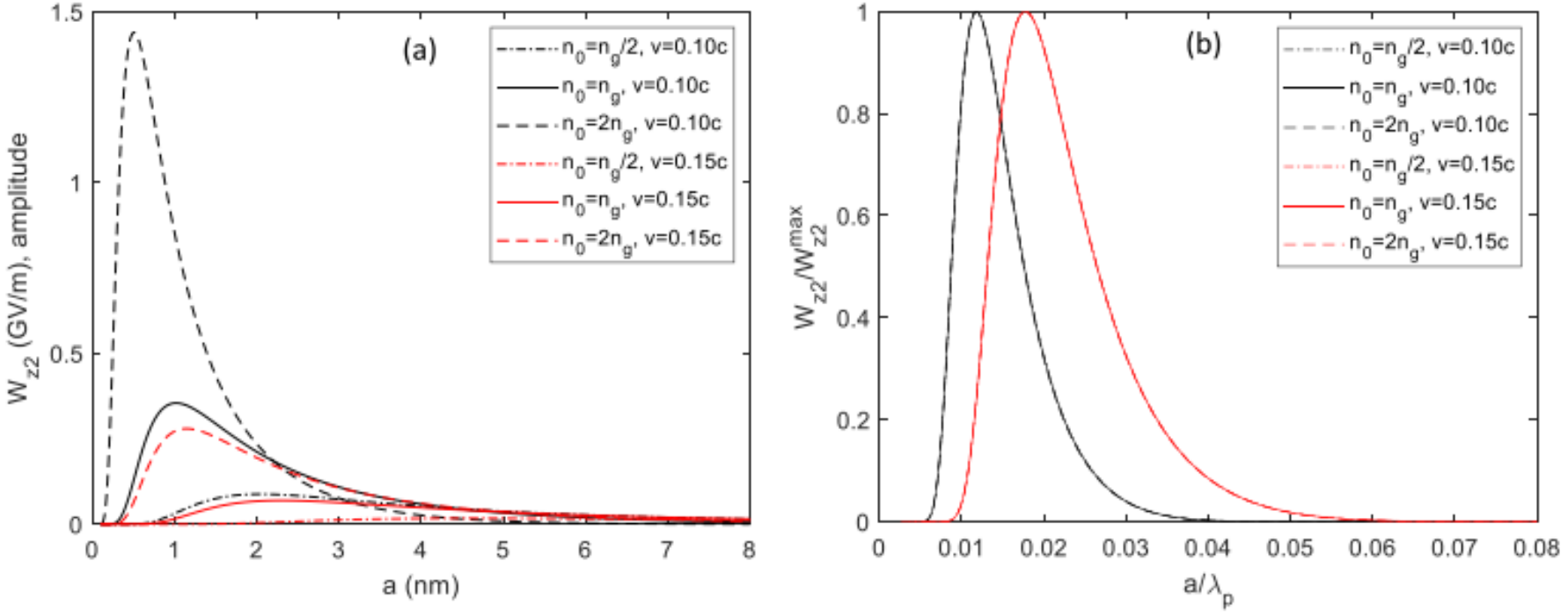

Figure 8. (a) Amplitude of W_{z2} as a function of the radius a for different values of n_0 and v ($n_g = 1.53 \times 10^{20}$ m^{-2} is the electron-gas density of a graphite sheet). (b) Amplitude of W_{z2} (normalized to the maximum of figure (a)) as a function of a/λ_p.

https://doi.org/10.1088/1367-2630/ad127c

3. Results

- **Optimization of CNT parameters:**

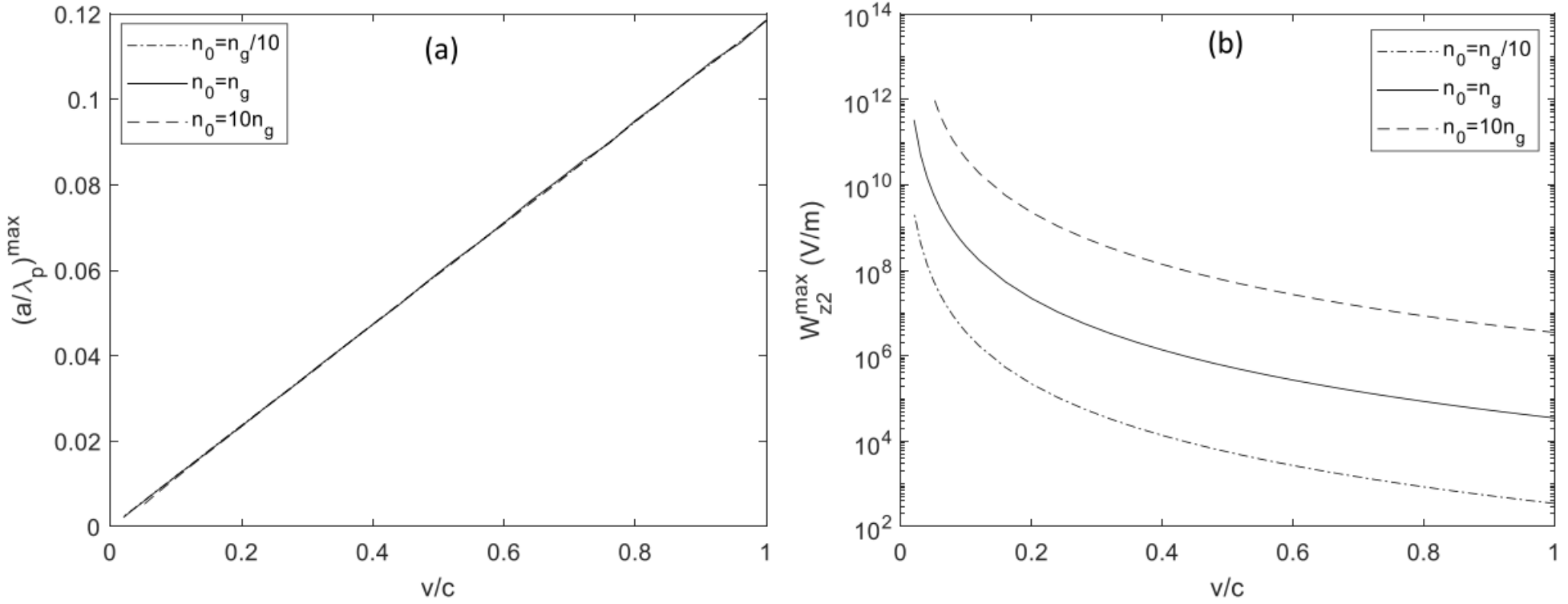

Figure 9. (a) Optimum radius and (b) maximum longitudinal wakefield associated as a function of v for different surface densities ($n_g = 1.53 \times 10^{20}$ m^{-2} is the electron-gas density of a graphite sheet).

Driving particles with low velocities may excite higher wakefields. A single ultrarelativistic proton may excite longitudinal wakefields in the order of 0.1 MV/m -> Bunches with milions of protons: 0.1 TV/m

https://arxiv.org/abs/2401.08334

3. Results (DWCNT)

- **Resonant frequencies:**

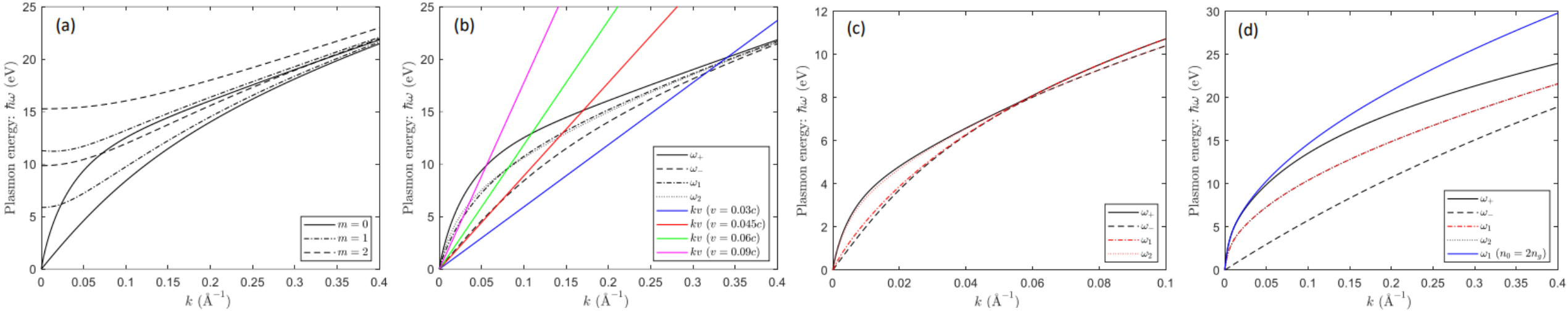

Figure 2. (a) Dispersion curves $\omega_\pm(m,k)$ for several angular-momentum modes for $a_1 = 1\,\text{nm}$ and $a_2 = 2\,\text{nm}$. (b) Fundamental modes $m = 0$ for $a_1 = 1\,\text{nm}$ and $a_2 = 2\,\text{nm}$ compared to the individual electron fluid frequencies ω_1 and ω_2. The resonances $k_0^\pm$ are the intersection of the kv lines (plotted for $v = 0.03c, v = 0.045c, v = 0.06c$ and $v = 0.09c$) with the dispersion curves. Fundamental modes $m = 0$ for (c) $a_1 = 1\,\text{nm}$ and $a_2 = 10\,\text{nm}$ and (d) $a_1 = 10\,\text{nm}$ and $a_2 = 10.34\,\text{nm}$ compared to the SWCNT frequencies ω_1 and ω_2.

Two resonant frequencies may be excited

https://arxiv.org/abs/2401.08334

3. Results (DWCNT)

- **Excited wakefields:**

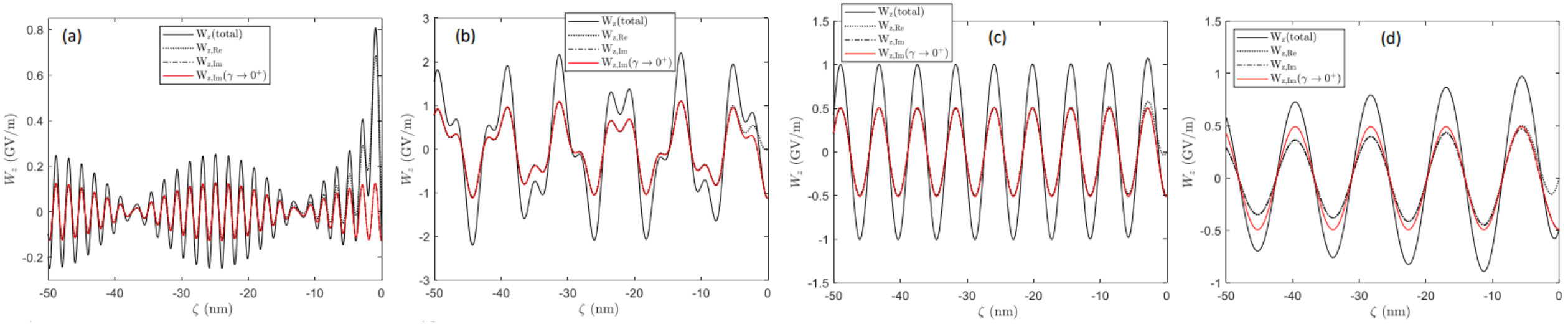

Figure 3. Induced longitudinal wakefield contributions on axis ($r = 0$) for a proton travelling on axis ($r_0 = 0$) at different velocity values: (a) $v = 0.03c$, (b) $v = 0.045c$, (c) $v = 0.06c$ and (d) $v = 0.09c$. The DWCNT radii are $a_1 = 1\,\text{nm}$ and $a_2 = 2\,\text{nm}$ and the friction parameter is $\gamma = 10^{-4}\Omega$ in cases (a)-(c), and $\gamma = 10^{-2}\Omega$ in (d), where $\Omega = \sqrt{4\pi n_0/a_1}$. The red curves show the approximation for small damping (Eq. (22)). Note that the driving proton is at the comoving coordinate $\zeta = 0$.

In cases (a)-(b) two resonant frequencies are excited. The total wakefields can be approximately by twice $W_{z,Im}$

https://arxiv.org/abs/2401.08334

3. Results (DWCNT)

- **Excited wakefields:**

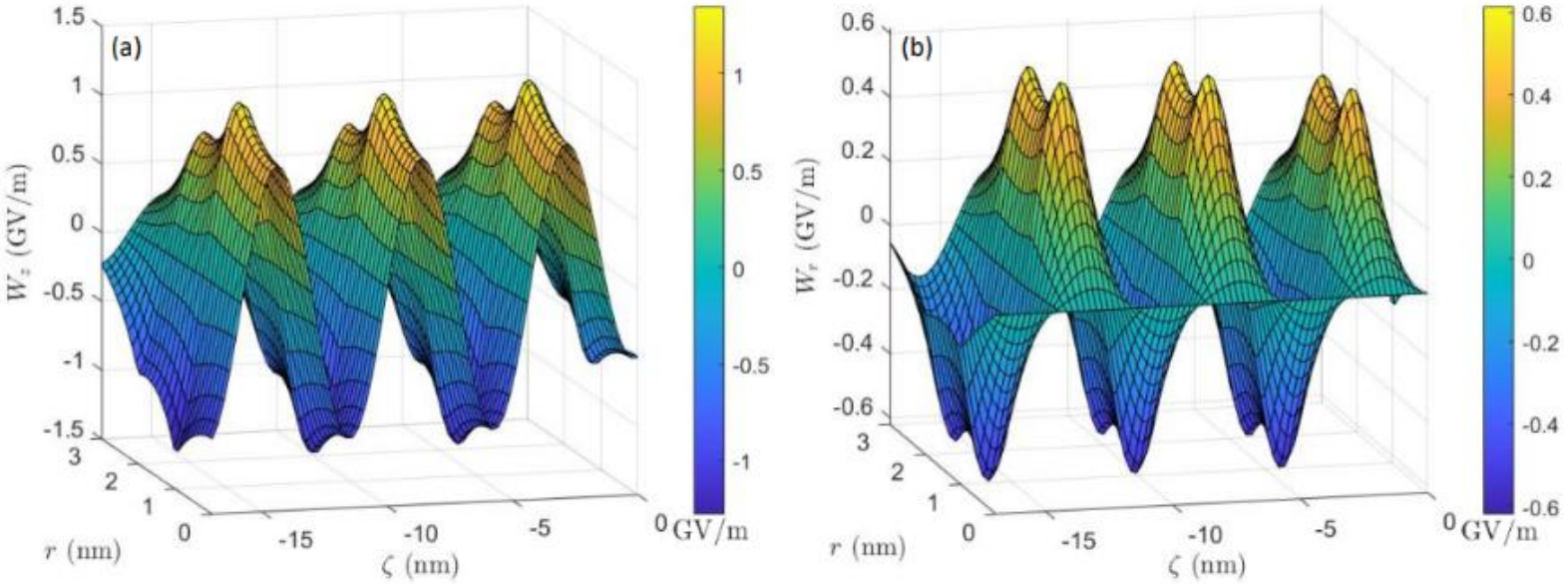

Figure 4. Induced (a) longitudinal and (b) transverse wakefields in the rz-plane generated by a driving proton travelling on-axis inside a DWCNT considering the following parameters: $a_1 = 1\,\text{nm}$ and $a_2 = 2\,\text{nm}$, $v = 0.06c$ and $\gamma = 10^{-4}\Omega$, where $\Omega = \sqrt{4\pi n_0/a_1}$.

The wakefields are higher near the walls

https://arxiv.org/abs/2401.08334

3. Results (DWCNT)

- **Contribution from each resonant frequency:**

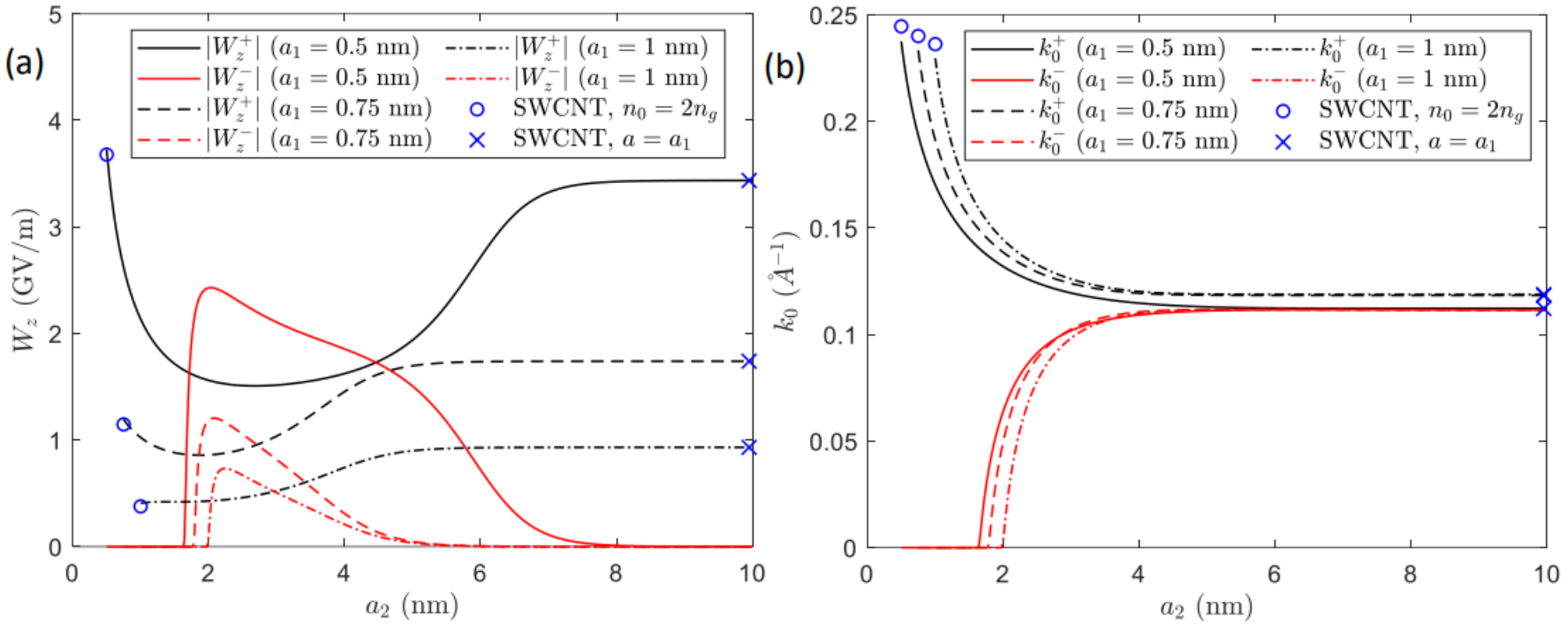

Figure 8. (a) Amplitudes $W_z^{\pm}$ and and (b) resonant wavenumbers $k_0^{\pm}$ as a function of the external radius a_2 for different a_1. The parameters used are: $v = 0.05c$ and $r = r_0 = 0$. The results are compared with the case of a SWCNT with $a = a_1$ and $n = 2n_g$ (circles) and a SWCNT with $a = a_1$ and $n = 2n_g$ (crosses) (Eq. (15) in [13]).

https://arxiv.org/abs/2401.08334

3. Results (DWCNT)

- **Scan in radius for a given inter-wall distance:**

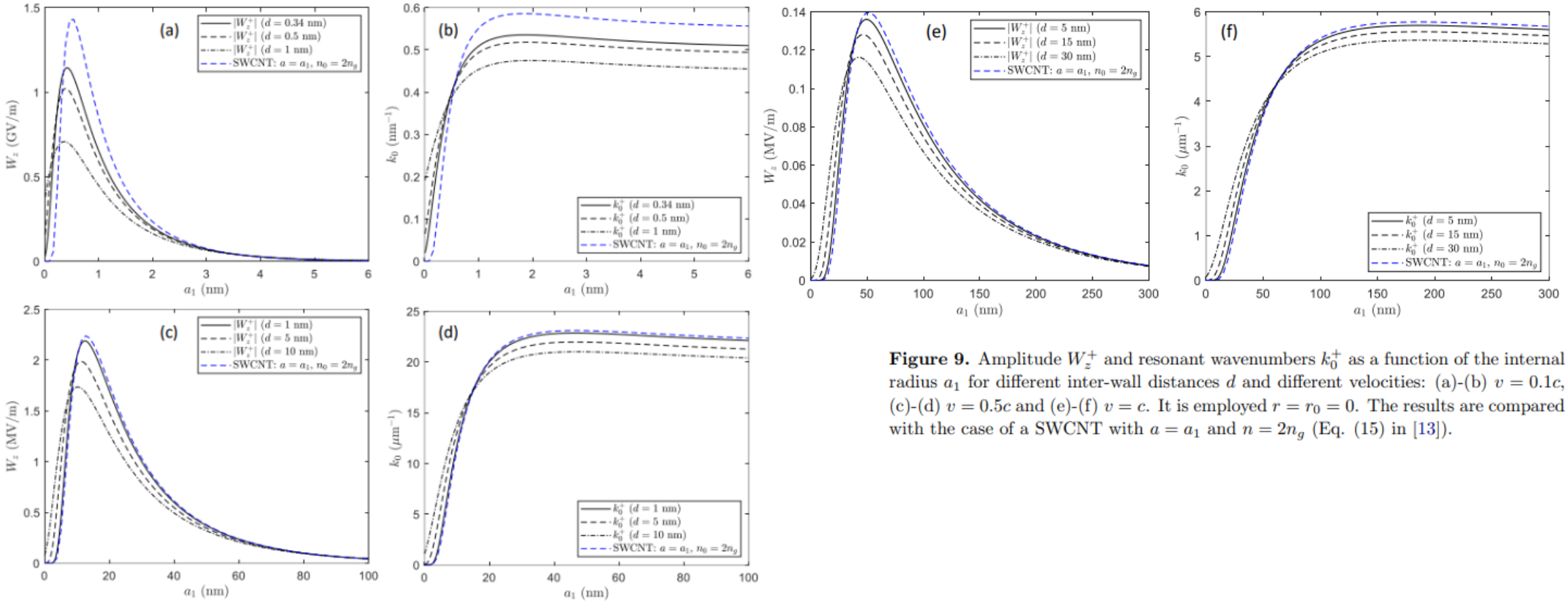

Figure 9. Amplitude W_z^+ and resonant wavenumbers k_0^+ as a function of the internal radius a_1 for different inter-wall distances d and different velocities: (a)-(b) $v = 0.1c$, (c)-(d) $v = 0.5c$ and (e)-(f) $v = c$. It is employed $r = r_0 = 0$. The results are compared with the case of a SWCNT with $a = a_1$ and $n = 2n_g$ (Eq. (15) in [13]).

DWCNTs with large a1 and small d can be optimised to obtain the highest wakefields employing the expressions for SWCNTs, but using n0 = 2ng. Such as in the case of SWCNTs with higher surface density n0, in which larger wakefields can be achieved, DWCNTs with small inter-wall distances can be used to obtain higher wakefields.

4. Conclusions and outlook

- We have presented a **linear hydrodynamic model for wakefield excitation** by charges in multi-walled nanotubes.
- A driver particle can excite **plasmons** in nanotubes.
- In the **limit $\gamma \rightarrow 0^+$** we can **calculate easily the excited wakefield** and the dependences on the different parameters, which allows to perform a fast optimization of the CNT parameters.
- **All the calculations** have been made for the **mode m=0** (since if r0=0 is the only mode excited). **Higher modes are less important**, but they are not negligible if the driver is off-axis near to the surface.
- The results show **>GV/m fields** and are **qualitatively similar to the PIC simulations** and the order of magnitude is similar. Systematic comparisons with PIC simulations are ongoing.
- Published papers (SWCNTs): https://doi.org/10.1088/1367-2630/ad127c (New J. Phys.), https://iopscience.iop.org/article/10.1088/1742-6596/2687/4/042005/meta (*J. Phys.: Conf. Ser.)*
- Submitted paper to *Results in Physics* about DWCNTs: https://arxiv.org/abs/2401.08334

Contents (PMTs)

1. Introduction
2. Simulations
3. Conclusions and ongoing work

1. Introduction

- Photomultiplier tubes (PMTs) are widely deployed as photodetectors thanks to their robustness and sensitivity.
- The description of the PMT response to incident light is usually limited to effective models, that describe the amplification of light into a measurable electric signal with analytical equations.
- These models do not take into account the geometry of the dynodes.
- The effect on the PMT gain of e.g. magnetic fields, non-linear response with high light intensity or space charge effects can only be described from a qualitative or even speculative point of view.

- Main goals of this study:
  - To simulate the amplification and transport of electrons in a real PMT geometry.
  - To validate the simulation and calibrate its parameters based on experimental measurements of the PMT gain.

2. Simulations

- **PMT structure:**

Table 1
Recommended voltage ratios between cathode, grid, dynodes, Acc and anode of the ø1.5" R13408-100 PMT.

Electrodes	Cathode	Grid	Dy1	Dy2	Dy3	Dy4	Dy5	Dy6	Dy7	Dy8 (Acc)	Anode
Ratio	1.3		4.8	1.5	1.5	1	1	1	1	1	1

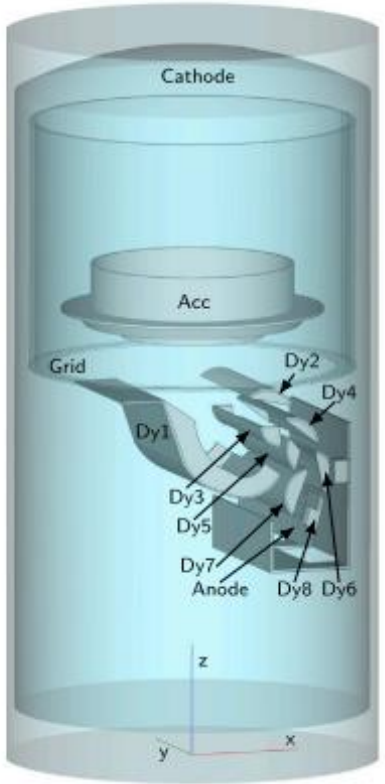

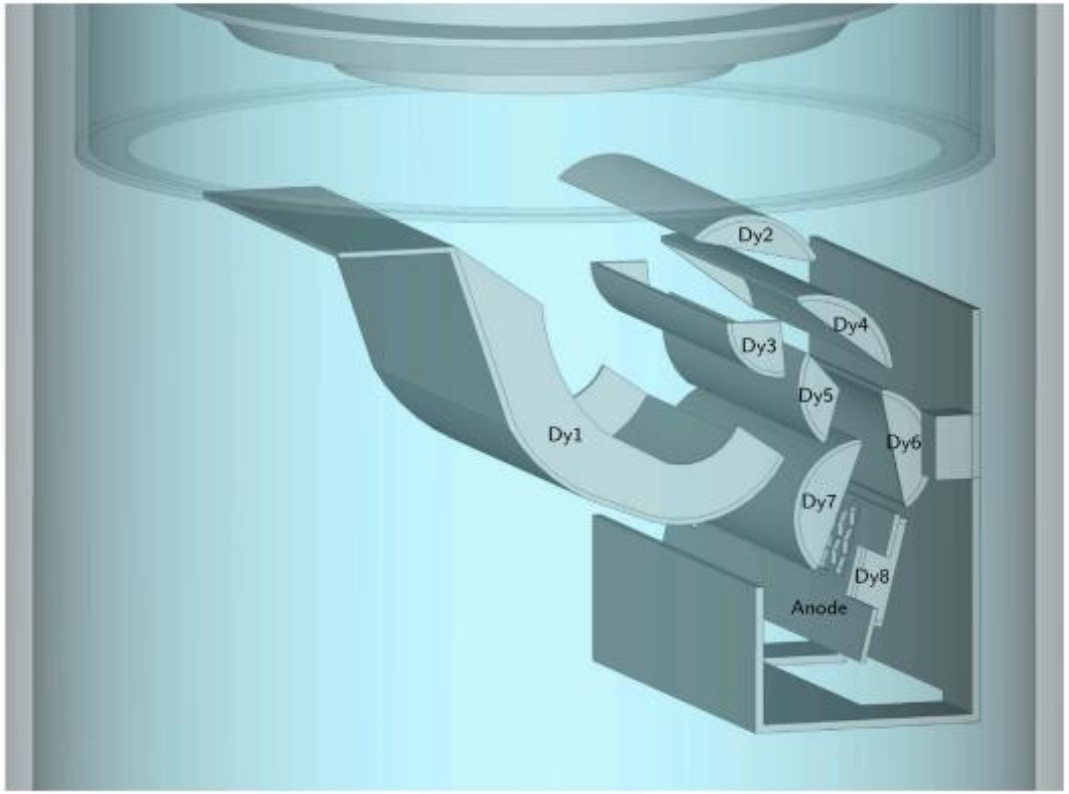

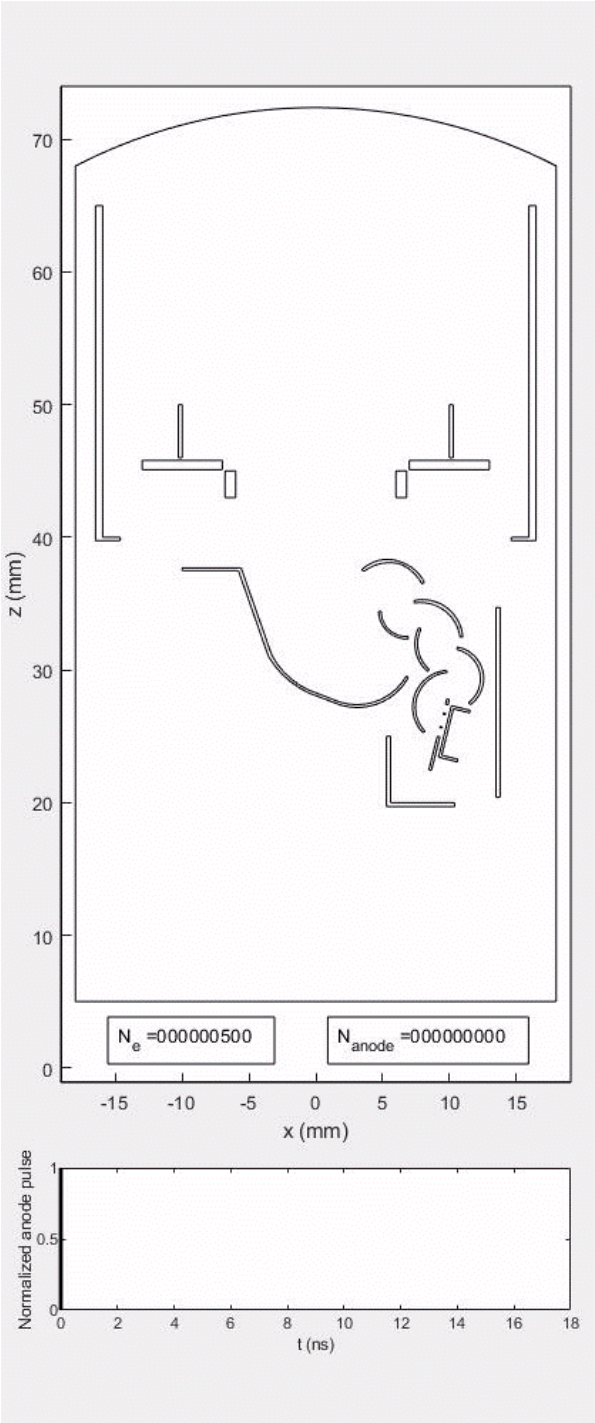

https://doi.org/10.1016/j.sna.2023.114859

https://doi.org/10.1016/j.sna.2023.114859

2. Simulations

- **Results: Supply Voltage**

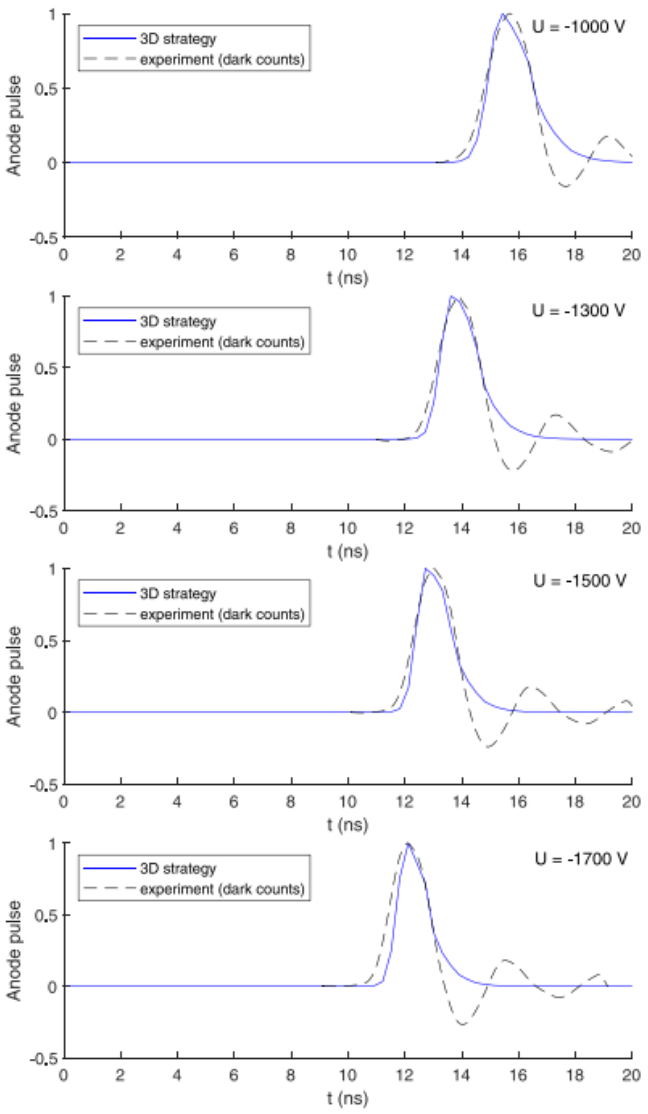

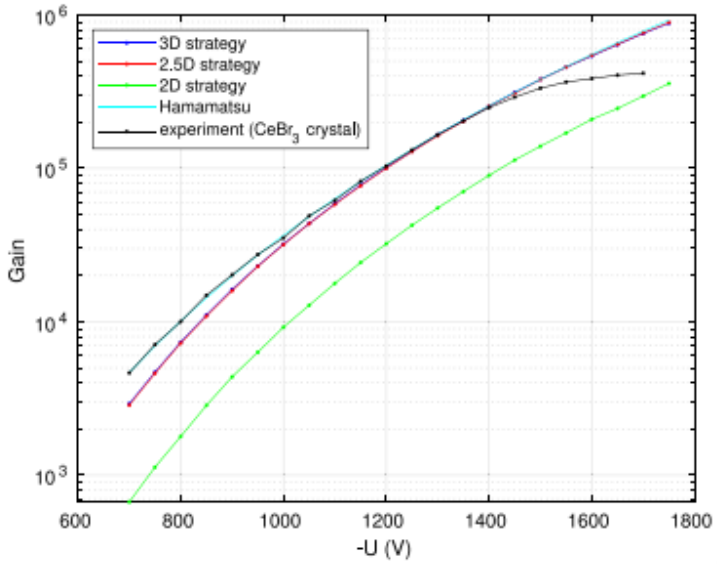

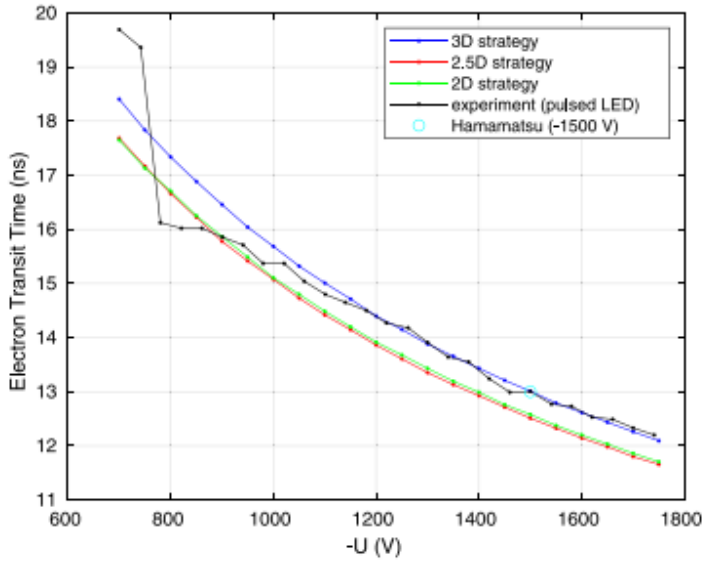

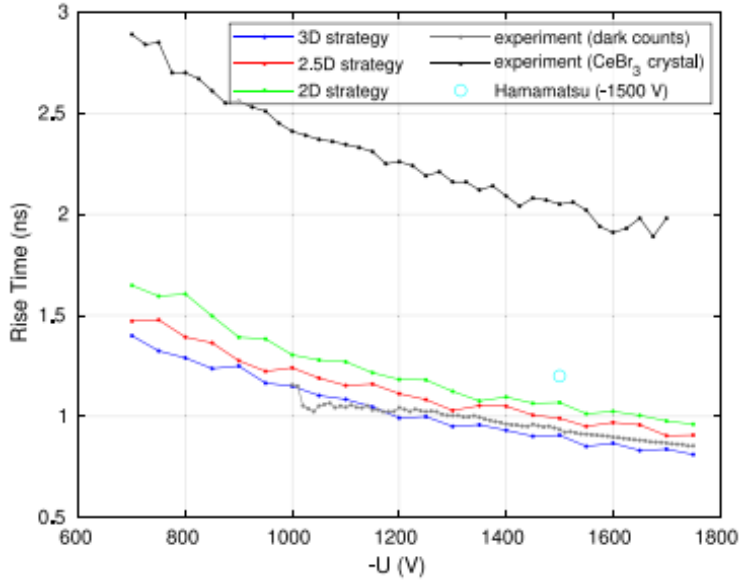

https://doi.org/10.1016/j.sna.2023.114859

2. Simulations

- **Results: External magnetostatic field**

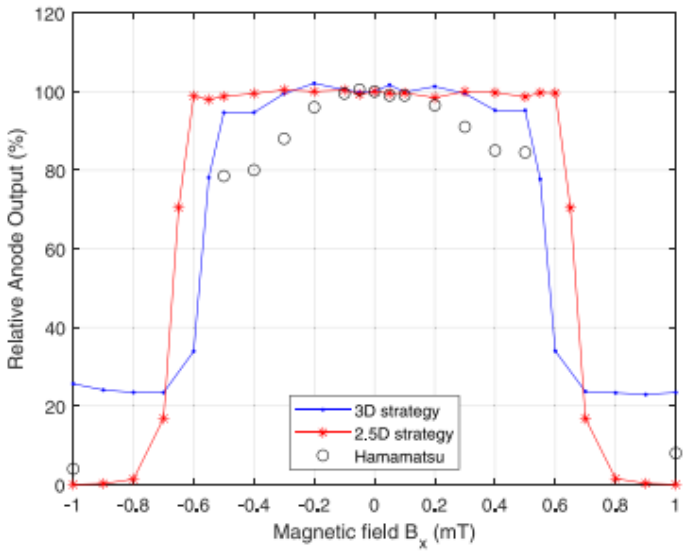

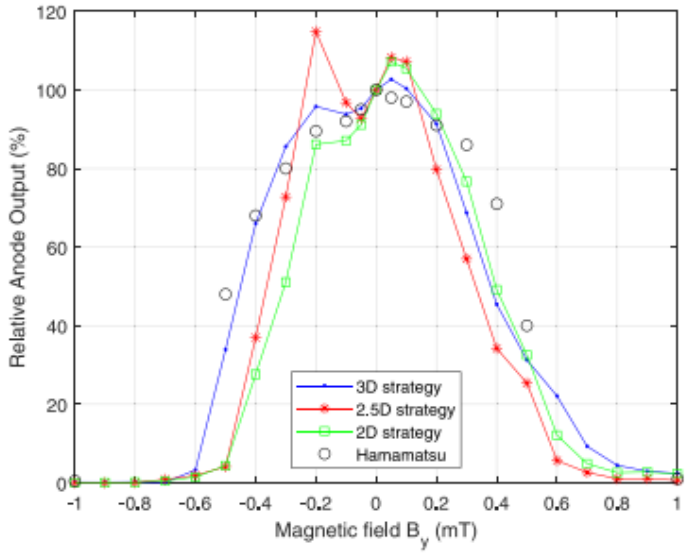

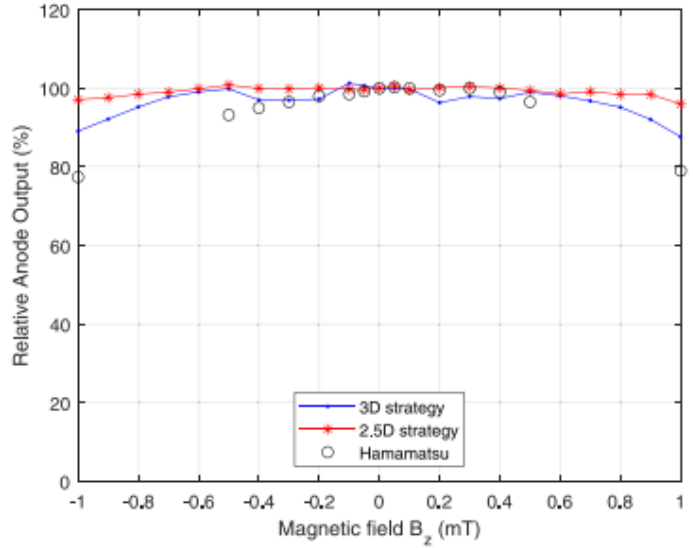

3. Conclusions and ongoing work

- The simulation of the PMT using its geometry shows a **good agreement** with the experimental measurements for a wide range of voltages.
- The 2.5D strategy is a good approximation with a much lower computational cost compared to the 3D strategy.
- Published paper in Sensors and Actuators A: https://doi.org/10.1016/j.sna.2023.114859

- To study the discrepancies obtained, the **ongoing** and **future work** is based on:
  - The effect of the electrode currents flowing into the passive divider network, in particular for higher voltages.
  - Study of the space charge instead of effective model.

Acknowledgments

- This work is supported by Ministerio de Universidades (Gobierno de España) under grant number FPU20/04958 and the Generalitat Valenciana under grant number CIDEGENT/2019/058.